ACS Catalysis

pubs.acs.org/acscatalysis

Research Article

Dual-Site-Mediated Hydrogenation Catalysis on Pd/NiO: Selective Biomass Transformation and Maintenance of Catalytic Activity at Low Pd Loading

Sebastiano Campisi, Carine E. Chan-Thaw, Lidia E. Chinchilla, Arunabhiram Chutia, Gianluigi A. Botton, Khaled M. H. Mohammed, Nikolaos Dimitratos, Peter P. Wells,* and Alberto Villa*

Cite This: *ACS Catal.* 2020, 10, 5483−5492

Read Online

ACCESS | Metrics & More | Article Recommendations | Supporting Information

ABSTRACT: Creating a new chemical ecosystem based on platform chemicals derived from waste biomass has significant challenges: catalysts need to be able to convert these highly functionalized molecules to specific target chemicals and they need to be economical—not relying on large quantities of precious metals—and maintain activity over many cycles. Herein, we demonstrate how Pd/NiO is able to direct the selectivity of furfural hydrogenation and maintain performance at low Pd loading by a unique dual-site mechanism. Sol-immobilization was used to prepare 1 wt % Pd nanoparticles supported on NiO and TiO_2, with the Pd/NiO catalyst showing enhanced activity with a significantly different selectivity profile; Pd/NiO favors tetrahydrofurfuryl alcohol (72%), whereas Pd/TiO_2 produces furfuryl alcohol as the major product (68%). Density functional theory studies evidenced significant differences on the adsorption of furfural on both NiO and Pd surfaces. On the basis of this observation we hypothesized that the role of Pd was to dissociate hydrogen, with the NiO surface adsorbing furfural. This dual-site hydrogenation mechanism was supported by comparing the performance of 0.1 wt % Pd/NiO and 0.1 wt % Pd/TiO_2. In this study, the 0.1 and 1 wt % Pd/NiO catalysts had comparable activities, whereas there was a 10-fold reduction in performance for 0.1 wt % Pd/TiO_2. When TiO_2 is used as the support, the Pd nanoparticles are responsible for both hydrogen dissociation and furfural adsorption and the activity is strongly correlated with the effective metal surface area. This work has significant implications for the upgrading of bioderived feedstocks, suggesting alternative ways for promoting selective transformations and reducing the reliance on precious metals.

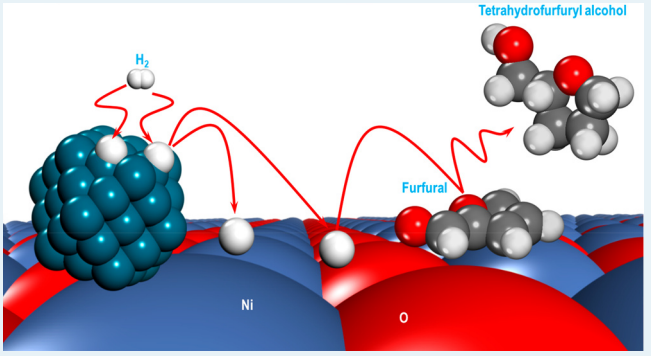

KEYWORDS: *furfural hydrogenation, Pd, NiO, heterogeneous catalysis, hydrogen spillover*

INTRODUCTION

To expedite the transition from a chemical ecosystem based on petroleum to one based on sustainable bioderived platform chemicals requires a concerted effort: catalysts need to (i) be highly active under mild conditions, (ii) be atom efficient and achieve a high selectivity to a desired product, (iii) maintain performance over many cycles, and (iv) be economical by not relying on large amounts of scarce and expensive metals. These objectives necessitate detailed catalytic studies that probe the performance on an atomistic level and are able to describe how specific materials promote these complex transformations.

In this regard, there have been significant efforts to understand the transformation of lignocellulosic biomass to fine chemicals and fuels.[1−3] Furfural, derived from the hydrolysis of the hemicellulosic fraction of lignocellulose, is considered as a viable platform molecule to many value-added products (Scheme 1).[4,5] Furfuryl alcohol (FA), obtained via hydrogenation of the furfural carbonyl group, is widely used for producing resins, lubricants, plasticizers, and fibers.[6,7] The hydrogenation of both the carbonyl group and furanic ring produces tetrahydrofurfuryl alcohol (THFA), a green solvent used in printer inks and agriculture applications.[8] In spite of the relevance of these compounds, furfural hydrogenation presents a complex pathway, requiring tailored catalysts to direct the selectivity toward the desired products.

To optimize the hydrogenation reaction of furfural, many noble-metal catalysts have been studied.[9] Pd and Ir lead to the formation of FA as the main product,[10,11] whereas Ni promotes selectivity to THFA.[12] The product distribution

Received: January 24, 2020
Revised: April 9, 2020
Published: April 10, 2020

https://dx.doi.org/10.1021/acscatal.0c00414
ACS Catal. 2020, 10, 5483−5492

Scheme 1. Chemical Routes for Furfural Valorization

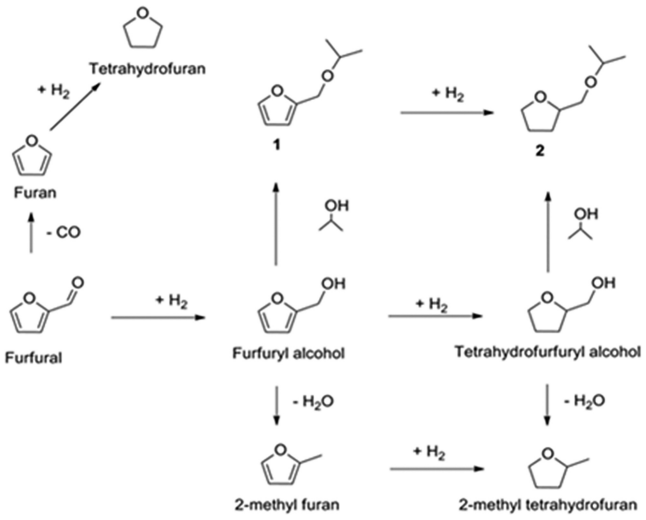

depends on the affinity of the reactant for the metal, as well as the preferential mode of adsorption on specific sites (e.g., steps, edges, corners, and terraces) of the catalyst.[9,13] A perpendicular adsorption, through the carbonyl group, results in the formation of furfuryl alcohol and 2-methylfuran.[6,14] A flat adsorption, through the furanic ring and carbonyl functionality, produces THFA.[15] At high temperature, a flat orientation results in the decarbonylation of furfural, producing furan and tetrahydrofuran.[7,16] A strategy for tuning the selectivity is to selectively block these specific active sites on the metal surface using thiolates or polymers such as poly(vinyl alcohol) (PVA);[17−19] the latter of these has a dual purpose, as it is commonly used to limit the growth of colloidal Pd nanoparticles during sol-immobilzation.[18] However, the effects of the metal sites on directing the transformation of highly functionalized bioderived substrates to specific products cannot be assessed in isolation; the support material is not benign and has a significant influence on the catalytic properties.[20−22] The "so-called" strong metal−support interactions (SMSIs) at the interface are responsible for electron transfer, charge redistribution, morphological changes, metal decoration or encapsulation, metal−support borderline site creation, and spillover phenomena.[23−25] Furthermore, the supports themselves are involved in catalytic transformations either in isolation or in tandem with supported metal nanoparticles.[26] Indeed, sea urchin like NiO was recently demonstrated to possess excellent catalytic activity in the selective hydrogenation of furfural to FA.[27] The mechanism for the enhancement enabled by the metal−support interaction is very specific—for both the metal/metal oxide combination and the reaction under study. For furfural hydrogenation, Somorjai et al. used sum frequency generation (SFG) vibrational spectroscopy to reveal the role of O vacancies at the metal support perimeter in determining the distribution of products over Pt/TiO_2 catalysts.[28] Elsewhere, Seemala et al. demonstrated that different supports (Al_2O_3 and TiO_2) induce different surface compositions of bimetallic Cu−Ni and therefore different activities in furfural hydrogenation.[14]

It is clear that tailoring the properties of both the metal nanoparticles and the support has profound consequences for the resultant performance toward the hydrogenation of furfural. In this study, our combined experimental and theoretical approach demonstrates how Pd/NiO not only directs the selectivity of furfural hydrogenation but also operates through a unique dual-site hydrogenation mechanism that allows for high catalytic activity to be maintained at low (0.1 wt %) Pd loading.

EXPERIMENTAL SECTION

Catalyst Synthesis. *NiO Preparation.* Nickel(II) nitrate hexahydrate (0.134 M, $Ni(NO_3)_2{\cdot}6H_2O$, Sigma-Aldrich, purity >99.9%) and urea (Sigma-Aldrich, purity >99.5%) (Ni/urea molar ratio 1/12 mol/mol) were solubilized and mixed in 0.2 L of water with magnetic stirring for 240 min at 80 °C. The suspension was filtered to separate the precipitated nickel hydroxide, $Ni(OH)_2$, from the solution. The powder was washed with 2 L of water, dried at 100 °C for 120 min, and finally calcined at 300 °C for 60 min.

Pd Catalyst. A Pd(II) salt (0.051 mmol of Na_2PdCl_4, Sigma-Aldrich, purity >99.9%) was dissolved in 0.1 L of water and sequentially 1 mL of 1 wt % poly(vinyl alcohol) solution (Pd/PVA mass ratio 1/0.5 wt/wt) was introduced. The as-obtained yellow solution was maintained under vigorous magnetic stirring for 3 min, and then a precise volume of 0.1 M $NaBH_4$ solution ($Pd/NaBH_4$ molar ratio 1/8 mol/mol) was injected. Immediately, the solution assumed a brown coloration, indicating the formation of Pd(0) colloid. After a few minutes, sulfuric acid was added to adjust the pH to 2 and then the solid support was dispersed in the vigorously stirred colloid. The amount of the support was selected in order to achieve final palladium loadings of 1 and 0.1 wt % (on the assumption of a quantitative metal uptake on the support). After filtration and washing, the catalysts were dried at 100 °C for 120 min.

Catalytic Tests. Catalytic performances in the furfural (F; Sigma-Aldrich, purity 99%) hydrogenation reaction were evaluated at 25 °C, carrying out batch experiments in a stainless steel reactor (0.03 L capacity) equipped with a heater, mechanical stirrer, gas supply system, and thermocouple for temperature control. The reactor was filled with 0.015 L of furfural solution (0.3 M in 2-propanol), and the proper amount of catalyst (F/metal ratio 500 mol/mol) was suspended in the solution. The reactor was pressurized with 5 bar of pure hydrogen. The mixture was kept at room temperature (25 °C) with mechanical stirring (1250 rpm). At the end of the test, the gas flow was switched from H_2 to N_2 to purge the autoclave with flowing nitrogen. Periodic sampling (200 μL) allowed monitoring of the progress of the reaction by chromatographic analysis, using a HP 7820A gas chromatograph equipped with a 30 m × 0.32 mm, 0.25 μm film HP-5 capillary column, by Agilent Technologies. Compound identification was performed on the basis of retention times obtained from an analysis of authentic samples. An external standard method (*n*-octanol) was used for the quantitative analysis.

Transmission Electron Microscopy (TEM). Holey copper grids were used for performing TEM studies, where small quantities of powdered catalysts were deposited onto the grids prior to analysis. The TEM studies—for producing both images and elemental analysis through X-ray energy dispersive spectroscopy (XEDS)—were conducted in high annular dark field mode using a FEI Titan3 80-300 microscope. The acceleration voltage was 200 kV. All data were analyzed using the software packages Digital Micrograph, TIA, and INCA. Information on particle size distribution (PSD) assumed a truncated cuboctahedral particle shape and was assessed using Gauss software.

https://dx.doi.org/10.1021/acscatal.0c00414
ACS Catal. 2020, 10, 5483−5492

Table 1. Catalytic Activity Testing for the Hydrogenation of Furfural at 50 °C and TEM Particle Size Data[a]

		selectivity (%)[d]							Pd particle size[f]	
							ether			
catalyst[b]	activity[c]	FA	THFA	2-MF	2-MTHF	furan	1	2	median (nm)	deviation (nm)
TiO_2										
NiO	39	4[e]	87[e]					4[e]		
1% Pd/NiO	470	14	72	1	5	1		3	3.1	0.5
1% Pd/TiO_2	321	67	23			1	5		2.7	0.9

[a]Abbreviations: FA = furfuryl alcohol, THFA = tetrahydrofurfuryl alcohol, 2-MF = 2-methylfuran, 2-MTHF = 2-methyltetrahydrofuran. [b]Reaction conditions: furfural 0.3 M; F/metal ratio 500 mol/mol, 50 °C, 5 bar H_2, solvent 2-propranol. [c]Moles of furfural converted per hour per mole of metal, calculated after 15 min reaction: mol (metal mol)$^{-1}$ h^{-1}. [d]Selectivity at 60% conversion. [e]Selectivity at 10% conversion. [f]Calculated using 300 particles. Histograms are shown in Figure S5.

X-ray Photoelectron Spectroscopy (XPS). The acquisition of X-ray photoelectron spectra (XPS) was performed on a PHI 3056 XPS instrument with an Al anode source operated at 15 kV and an applied power of 0.35 kW. A sputter-cleaned silver foil was used for checking the energy scale calibration. Powders were hand-pressed between two clean slices of indium foil; the indium foil in which the powders were embedded was then placed in the sample holder with a fragment of carbon tape (Nisshin E.M. Co. Ltd.). The lowest C 1s binding energy species were shifted about 0.1 eV to 284.8 eV for comparison purposes with literature values. The XPS analyses did not require any pretreatments (i.e. cleaning, heating, and processing). High-resolution scans were acquired with a 23.5 eV pass energy and 0.05 eV steps a minimum of 50 times; survey scans were measured with a 93.9 eV pass energy and 0.5 eV energy steps a minimum of 25 times. Peak area integration provided surface concentrations, considering the proper standard atomic sensitivity factors provided by the instrument producer. Gaussian−Lorentzian functions and a Shirley-type background were used for spectral deconvolution.

X-ray Absorption Fine Structure (XAFS). Measurements were conducted at the U.K. national synchrotron Diamond Light Source, using the core-XAFS beamline B18. XAFS data at the Pd K edge were acquired simultaneously with a Pd-foil reference positioned between I_t and I_{ref}. Samples were prepared as self-supporting pellets and were assessed by fluorescence acquisition using a QEXAFS setup with a fast-scanning Si(311) double-crystal monochromator and a 36-element Ge detector. Each spectrum was measured for 4 min, and on average 6 scans were measured to improve the data quality of the final summed spectrum. Data were measured in K space to a maximum value of 16. Data processing was performed using IFEFFIT[29] with the Horae[30] packages (Athena and Artemis). The amplitude reduction factor S_0^2 was determined by analyzing a Pd foil and was determined to be 0.88 and used as a fixed input parameter.

Infrared CO Chemisorption Studies. A Nicolet is10 spectrometer was used for all Fourier transform infrared (FTIR) spectroscopy measurements. The spectral resolution was 2 cm^{-1}, and the total number of scans of the sample and the background was 64. All samples were measured in transmission as ultrathin self-supporting disks; approximately 25 mg of sample was used to form a disk of 13 mm diameter. A Harrick Dewar cell was used for the environmental studies. The sample environment was flushed with He for 30 min to obtain a background spectrum before CO was introduced using a 10% CO/90% He mixture at 70 mL min^{-1} over a 30 s period. There were three doses of CO for each experiment. Before a final spectrum was obtained, the gas was switched to helium for 30 min at 70 mL min^{-1}, in order to remove gaseous and physisorbed CO.

Atomic Absorption Spectroscopy (AAS). The palladium concentration on solid catalysts was determined by AAS analysis of the postsynthesis filtrate using a PerkinElmer 3100 instrument. For each catalyst, 0.01 L of the filtered solution was withdrawn and analyzed.

Powder X-ray Diffraction (XRD). X-ray diffraction patterns were collected on a PANalytical X'PertPRO X-ray diffractometer utilizing a Cu Kα radiation source (40 kV and 30 mA). XRD patterns were recorded in the 10−80° 2θ range over a scan time of 1 h.

DFT Studies. We used the Vienna ab initio simulation package (VASP) to perform all the spin-polarized periodic density functional theory based calculations.[31−33] The projector augmented wave (PAW) method was used, and a cutoff energy of 550 eV was employed for the expansion of the plane-wave basis sets, which gave bulk energies converged to within 10^{-5} eV.[34] For the structural optimization we chose a convergence criterion of 0.01 eV Å^{-1}, and a k-point grid of 3 × 3 × 1 was employed for all slab calculations. The Perdew−Burke−Ernzerhof (PBE) version of the generalized gradient approximation (GGA) was used to carry out geometry optimizations and the total energy calculations.[35] As the dispersive effects may be significant for the systems under consideration, we also used Grimme's dispersion correction (DFT+D3).[36] The ideal surfaces of Pd(111) and NiO(110) and rutile TiO_2(111) were modeled by a 4 × 4 cell with five atomic layers. Of the five atomic layers, the bottom three layers were fixed to mimic the bulk of the material; in the direction perpendicular to the surface we used a vacuum gap of ∼15 Å, which is sufficient to eliminate slab−slab interactions. The slabs were cut from bulk Pd, NiO, and rutile TiO_2 with a calculated energy minimized lattice constant of 3.904 Å (exptl 3.891 Å), 4.192 Å (exptl 4.168 Å), and 4.695 Å (exptl 4.594 Å), respectively. In all of the calculations, the adsorption of furfural was allowed on only one of the two exposed surfaces. The spurious dipole moment due to the adsorbed species was taken into account by using the methods implemented in VASP according to the procedures of Makov et al. and Neugebauer et al.[37,38] For the calculations on the interaction of furfural on the NiO(110) and TiO_2(111) surfaces we used DFT+U. Previous studies have shown that a U value of 5.77 eV, obtained by using linear response methods, for the d orbital of Ni is suitable.[39] It has been also reported that a U value of 4.20 eV is suitable for the d orbitals of Ti.[40] To determine the minimum energy paths for the dissociation of H_2 we employed the climbing-image nudged elastic band (CI-NEB) method. The transition state of the optimized reaction

https://dx.doi.org/10.1021/acscatal.0c00414
ACS Catal. 2020, 10, 5483−5492

coordinate was confirmed by calculations of the vibrational frequencies.

RESULTS

Pd nanoparticles were supported on TiO_2 (P25, 50 m^2 g^{-1}) and NiO through an established sol-immobilization method with a loading of 1 wt %. The metal loading was confirmed by atomic absorption spectroscopy (AAS). The NiO support was prepared using an in-house method involving the precipitation of $Ni(OH)_2$ in aqueous solution, followed by subsequent calcination. The preparation resulted in a nanostructured NiO with a particle size of 6 nm and a surface area of 210 m^2 g^{-1}. The NiO phase was identified using XRD (Figure S1). X-ray photoelectron spectroscopy (XPS) analysis provided useful insight on the nature of Ni surface species (Figure S2). Ni $2p_{3/2}$ data disclosed the presence of two main peaks corresponding to different Ni species on the surface; the first peak centered around 854.5 eV is due to Ni^{2+}−O lattice species, while the second peak centered around 856.1 eV confirmed that $Ni(OH)_2$ was also formed at the surface (Figure S2). The oxidation state of surface species has been investigated by XPS. Comparison of Pd 3d XP spectra for Pd/TiO_2 and Pd/NiO (Figure S2) revealed that Pd is present in the metallic form in both cases with a similar percentage of Pd0 (85% and 88% for Pd/NiO and for Pd/TiO_2, respectively). The supported metal nanoparticle catalysts and bare supports were then evaluated for the hydrogenation of furfural under mild conditions (Table 1); furfural 0.3 M, furfural/Pd ratio 500 mol/mol, 5 bar H_2, 50 °C and 2-propanol as solvent. Prior to the catalytic evaluation the appropriate Pd/furfural molar ratio was established to ensure the catalytic performance was in the kinetic regime and was not mass-transport limited (Table S1). The catalytic activity testing demonstrated that the 1 wt % Pd/NiO catalyst exhibited superior activity in comparison to the 1 wt % Pd/TiO_2 (470 (metal mol)$^{-1}$ h^{-1} vs 321 (metal mol)$^{-1}$ h^{-1})—approximately a 50% increase in activity. Notably, not only was there a difference in activity but also there was also a pronounced change in the selectivity profile. The Pd/NiO catalyst had a preferential selectivity toward THFA (72%), whereas Pd/TiO_2 favored FA (67%). Catalytic performance testing of the bare supports was also performed as a control experiment. Here, under analogous testing conditions there was no observable conversion of furfural on TiO_2. However, NiO showed a minor level of activity (39 (metal mol)$^{-1}$ h^{-1}) with THFA found as the major product (87%). This observation is consistent with recent studies that have already proven that NiO is able to hydrogenate furfural in the absence of precious metals.[27] The time-online data for the catalytic testing (Figures S3 and S4) confirmed that Pd/NiO favors THFA over FA as the major product at all time points. However, there is a sharp increase in THFA selectivity as the conversion of furfural progresses. This arises because of sequential hydrogenation reactions and the transformation of isopropyl tetrahydrofurfuryl ether to THFA. To understand the difference in catalytic properties, a series of studies to establish the physicochemical properties of the Pd nanoparticles was performed; the intention was to establish whether the catalytic data could be accounted for solely by the changes to Pd or if there was a synergistic effect between the metal and support. The Pd nanoparticle size data was found using transmission electron microscopy (Table 1 and Figure S5).

The Pd/TiO_2 and Pd/NiO catalysts were found to have comparable Pd particle sizes of 2.7 and 3.1 nm, respectively. Considering that smaller Pd nanoparticles have a larger available surface area, the difference in catalytic activity cannot be rationalized by this effect. In this instance, the catalyst with larger particles, and therefore smaller surface area, has the greatest catalytic activity. To probe the properties of the supported nanoparticles in further detail, a high-angle annular dark-field scanning TEM (HAADF-STEM) study was performed (Figure 1). The Pd/TiO_2 catalyst has been

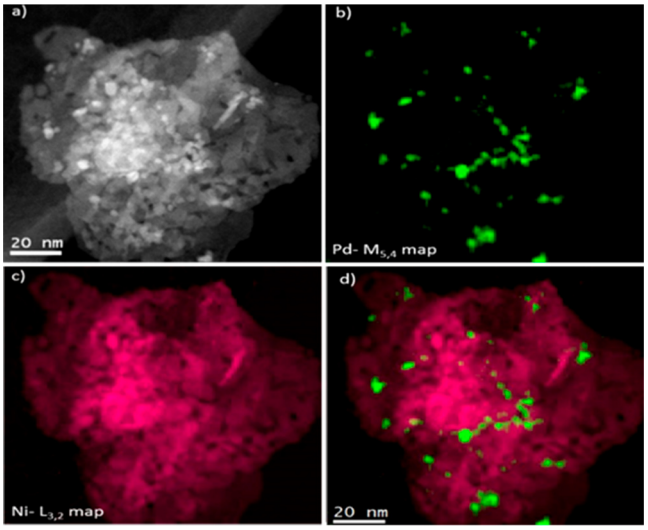

Figure 1. Representative low magnification STEM-HAADF images of Pd-NiO catalyst: (a−d) montage of HAADF image of Pd particles showing the corresponding EELS elemental maps and RGB reconstructed overlay maps (green, Pd; pink, Ni).

characterized previously by HAADF-STEM with the data being reported elsewhere;[18] to summarize, the Pd NPs were found to exhibit a significant number of sub-nanometer "clusters", as was also found for Au NPs prepared using an analogous low-temperature sol-immobilization procedure.[40]

Figure 1a shows a representative HAADF-STEM image of the Pd/NiO catalyst. In HAADF imaging, the intensity is approximately proportional to the square of the atomic number of the scattering element and therefore provides information on the local composition. In Figure 1a, the Pd particles (Z = 46) are clearly revealed as bright features on the nickel oxide matrix ($Z \approx 36$). This interpretation was confirmed by using electron energy loss spectroscopy (EELS). The EELS maps (Figure 1b−d) illustrate the presence of well-dispersed Pd nanoparticles (Pd M4,5 map in green) on NiO (Ni $L_{3,2}$ map in pink). The NiO appears as a collection of agglomerated platelets with diameters between 20 and 30 nm. Atomic resolution STEM images of a selected area (Figure 2a) reveal a highly crystalline particle with multiple twinning planes and clearly resolved lattice planes with a d spacing of 2.26 Å. This is in agreement with the expected spacing of the (111) planes of face-centered-cubic Pd metal. Additionally, high-resolution HAADF-STEM (Figure 2b) provides evidence of the presence of a sub-nanometer species (marked by yellow circles). This is in agreement with previous HAADF-STEM studies on other supported nanoparticle catalysts prepared using low-temperature sol-immobilization.[18,41] Figure S6 shows the deconvolution of the EELS data into three

https://dx.doi.org/10.1021/acscatal.0c00414
ACS Catal. 2020, 10, 5483−5492

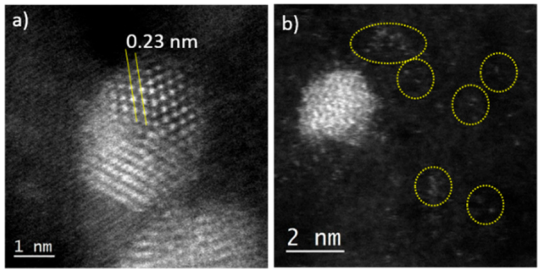

Figure 2. High-resolution STEM-HAADF images of 1 wt % Pd/NiO catalyst showing a crystalline particle (a) and sub-nanometer species of Pd distributed across the support (b).

components originating from the supporting NiO material (pink), the background (not shown), and the pure Pd particle (green). The features present could be assigned to the Pd $M_{4,5}$ edge (for Pd with onset at 335 eV), the oxygen K edge (onset at around 532 eV) and the Ni $L_{3,2}$ edge (at 855 eV).

Although the particle size is a valuable descriptor for catalytic activity, there are other effects to consider. Notably, the distribution of discrete sites on metal nanoparticle surfaces and their inherent ability to promote catalytic transformations are also of significant importance. The surface characteristics of the Pd/TiO_2 and Pd/NiO catalysts were assessed by a combination of CO adsorption and Fourier transform infrared (FTIR) spectroscopy (Figure 3).

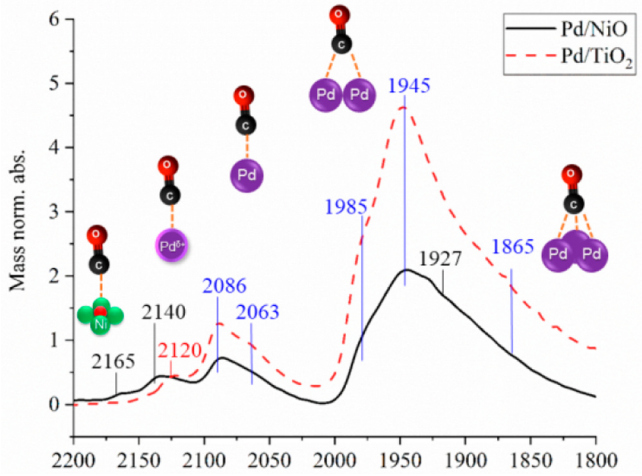

Figure 3. CO adsorption FTIR studies for Pd/NiO (black line) and Pd/TiO_2 (red line). Peaks assigned in blue are present in both catalysts, with those in red and black assigned solely to Pd/NiO and Pd/TiO_2, respectively.

Before assignment of the vibrational absorption bands on both catalysts there is a clear difference between the intensity of the absorption spectra; the data are normalized to mass of Pd, and the reduced intensity for the Pd/NiO data is indicative of a smaller available Pd surface area in agreement with the TEM data. The signals at 2120 and 2086 cm^{-1} are ascribed to CO linearly bound to Pd^+ and Pd particle corners, respectively.[42] The signal at 1985 cm^{-1} is related to bridge-bonded CO on Pd facets, whereas that at 1945 cm^{-1} is attributed to bridge-bonded CO on Pd edges.[42] The shoulder at 1865 cm^{-1} can be assigned to 3-fold sites.[43] The spectrum of 1 wt % Pd/NiO has additional bands at 2165, 2140, and 1927 cm^{-1}. The band at 2165 cm^{-1} is attributable to CO adsorption on NiO,[44] with the band at 1927 cm^{-1} assigned to bridge-bonded CO on Pd facets.[45] The FTIR spectra with CO probe molecule adsorption do not reveal profound differences in the surfaces of the Pd nanoparticles of both catalysts. Previously, the ratio of linear to bridge-bonded CO has been used to infer the likelihood of parallel or perpendicular furfural adsorption and then correlated to the selectivity of furfural hydrogenation. In the spectra presented in Figure 3, there are only minor differences in the linear/bridged ratio (0.28 and 0.32 for Pd/NiO and Pd/TiO_2, respectively), which confirms that the observed difference in selectivity for the hydrogenation of furfural is not linked to the surface characteristics of the Pd nanoparticles. This observation led to the hypothesis that there are distinct mechanistic pathways for both catalysts that are directed by differences in the metal−support interaction.

To probe the effect of the support in greater detail, a density functional theory with dispersion correction (DFT+D3) study into the adsorption energetics of furfural on Pd(111), NiO(110), TiO_2(111), and Pd_{16}/NiO(110) was undertaken. We first compare the calculated adsorption energies (E_{ad}) for the interaction of furfural on Pd(111) and NiO(110) surfaces. All of the optimized structures of furfural on Pd(111) and NiO(110) surfaces are shown in Figures S7 and S8. Our calculations show that the furfural molecule with a slanted configuration is more stable on the NiO(110) surface (E_{ad} = −2.572 eV) in comparison to its adsorption on the Pd(111) surface (E_{ad} = −1.649 eV) with a parallel configuration. Previous studies have also shown that the parallel configuration of furfural on the Pd(111) surface is more stable than its other possible orientations, and our calculated adsorption energy value for the adsorption of furfural on the Pd(111) surface is comparable with the previously reported values.[18,46−48] In the former case, the furanic ring is adsorbed via the O and C atoms of the −CHO group and O atom of the furanic ring (see Table S2), but in the latter, the interaction is via the C atoms of the furanic ring and the O atom of the −CHO group. Similar calculations were also performed on TiO_2(111) and on a single atomic layer of Pd adsorbed on the NiO(110) surface: i.e., Pd_{16}/NiO(110) (Figures S9 and S10 and Table S3). On the TiO_2(111) surface it is seen that the furfural molecule has a unique mode of interaction; it is adsorbed through two C atoms of the furanic ring with two O atoms on the surface, leaving the −CHO group noninteractive with the TiO_2(111) surface. On the other hand, the adsorption of furfural on Pd_{16}/NiO(110) is via the furanic C and aldehydic C and O atoms. The calculated adsorption energies of the furfural molecule on TiO_2(111) and Pd_{16}/NiO(110) are −4.113 and −1.946 eV, respectively. Figure 4 shows the most stable structures of furfural on Pd(111), NiO(110), TiO_2(111), and Pd_{16}/NiO(110) surfaces.

The DFT study confirmed distinct differences in the nature of furfural adsorption on Pd, TiO_2, NiO, and Pd_{16}/NiO systems. These observations, in combination with the selectivity profile of bare NiO, suggested that the difference in activity is associated with how NiO is able to activate furfural. In this scenario, it was hypothesized that the sole role of Pd on the Pd/NiO catalyst is to dissociate hydrogen. This hypothesis is consistent with recent hydrogenation studies on Ru/NiO/$Ni(OH)_2$/C catalysts, where an analogous mechanism was proposed.[49] Considering the facile nature of hydrogen dissociation, $E_{barrier}$ = 0.030 and 0.854 eV for the reverse reaction, which agrees well with our previous studies[50] (see Figure S11) over Pd surfaces. Therefore, this process

https://dx.doi.org/10.1021/acscatal.0c00414
ACS Catal. 2020, 10, 5483−5492

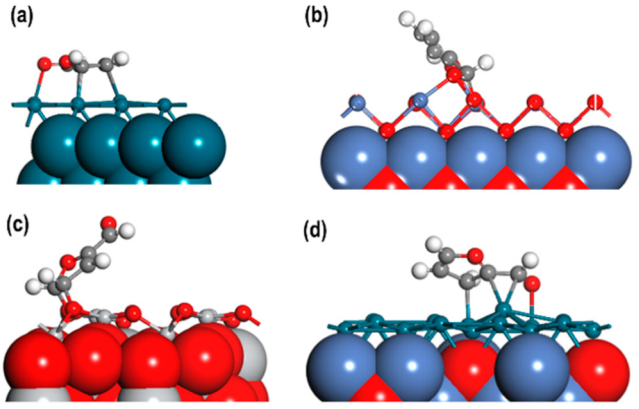

Figure 4. Optimized structures of furfural adsorbed on (a) Pd(111), (b) NiO(110), (c) TiO_2(111) and (d) Pd_{16}/NiO(110) surfaces. For clarity, the furfural molecule and the first two layers of the surfaces are shown as balls and sticks and the lower layers are shown in the CPK format.

would not be expected to be rate limiting. By extension, the catalytic activity would not have a linear correlation with the Pd metal loading (surface area): i.e., fast hydrogen dissociation on Pd surfaces, with slower hydrogenation of furfural on NiO surfaces. To test this hypothesis, two further catalysts were prepared, −0.1 wt % Pd/TiO_2 and 0.1 wt % Pd/NiO. The Pd loading was confirmed using AAS and the particle size assessed by HRTEM. The 0.1 wt % Pd/TiO_2 and 0.1 wt % NiO catalysts were found to have particle sizes of 2.2 and 3.8 nm, respectively (Figure S12).

The lower loading supported Pd catalysts were assessed using the same testing procedure reported earlier with the data presented in Table 1. The 0.1 wt % Pd/TiO_2 catalyst had an activity of 31 mol (metal mol)$^{-1}$ h^{-1}, an approximate 10-fold reduction in performance in comparison to that of the 1 wt % Pd/TiO_2 catalyst (321 mol (metal mol)$^{-1}$ h^{-1}) (Table 2). For the Pd/TiO_2 catalysts, both the hydrogen dissociation and furfural adsorption happen on the Pd surface. As the Pd loading decrease,s there is concomitant and, in this case, equal reduction in Pd surface area and as a consequence the rate of turnover. Conversely, the 0.1 wt % Pd/NiO catalyst shows only a minor loss of activity in comparison to the 1 wt % Pd/NiO catalyst: −421 mol (metal mol)$^{-1}$ h^{-1} vs 471 mol (metal mol)$^{-1}$ h^{-1}. The inference is that the hydrogenation mechanism of furfural is indeed different on Pd/NiO in comparison to Pd/TiO_2. This supports the proposed hypothesis that the role of Pd is to dissociate hydrogen and that the role of NiO is to bind and activate the substrate. It is worth stating that a minor amount of hydrogenation of furfural on the Pd surface is also possible, as is suggested by the subtle change in selectivity profile in comparison to NiO. However, seeing as the activity is maintained at such low Pd loadings, it would infer that the vast majority of furfural hydrogenation occurs on the NiO.

A further series of control experiments were then performed to assess the hydrogen spillover in greater detail. Initially, the catalytic activity of a physical mixture of 1 wt % Pd/TiO_2 and NiO was assessed; the intention was to confirm that the enhancement afforded by the NiO support was linked to the Pd−NiO interaction. The catalytic activity of the physical mixture proved different from that of the Pd/TiO_2 alone. The activity increased from 321 to 436 (metal mol)$^{-1}$ h^{-1}, a value greater than the addition of the activity of both separate components (1 wt % Pd/TiO_2 and NiO). Furthermore, there was also a change in the selectivity to THFA, increasing from 23 to 33%. The enhancement observed for the physical mixture of 1 wt % Pd/TiO_2 and NiO can be explained by the detachment of Ni during the hydrogenation reaction, which decorate Pd nanoparticles as found with HAADF STEM EDX studies (Figure 5). To assess further, whether this increase in performance could be a result of long-range hydrogen spillover, a control experiment of the 0.1 wt % Pd/TiO_2 with NiO was also performed. Here, the physical mixture showed catalytic performance broadly consistent with that of the 0.1 wt % Pd/TiO_2, with no discernible increase in rate; the dissolution and readsorption of Pd are negligible at these low loadings, and so no promotional effect is observed. These two control

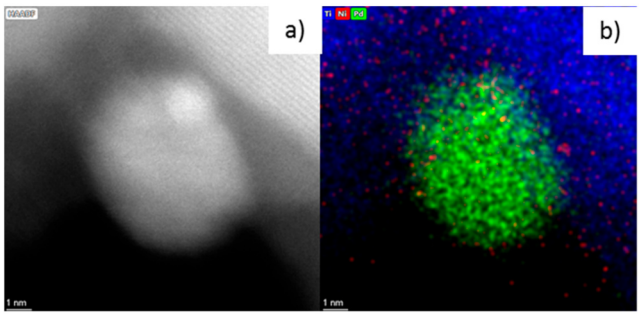

Figure 5. (a) STEM-HAADF image and (b) the corresponding elemental map from an individual particle of a physical mixture of 1 wt % Pd/TiO_2 and NiO after reaction.

Table 2. Catalytic Activity Testing for the Hydrogenation of Furfural at 50 °C and TEM Particle Size Data for Lower Loading of Pd/TiO_2 Catalysts and Control Experiments[a]

		selectivity (%)[d]							Pd particle size[f]	
							ether			
catalyst[b]	activity[c]	FA	THFA	2-MF	2-MTHF	furan	1	2	median (nm)	deviation (nm)
0.1% Pd/TiO_2	31	65[e]	20[e]	2[e]		2[e]	3[e]		2.2	0.4
0.1% Pd/TiO_2 + NiO	45	50	38	2		5	2			
1% Pd/TiO_2 + NiO	436	56	33		2		3	1		
0.1% Pd/NiO	421	10	81		7			1	3.8	1.2

[a]Abbreviations: FA = furfuryl alcohol, THFA = tetrahydrofurfuryl alcohol, 2-MF = 2-methylfuran, 2-MTHF = 2-methyltetrahydrofuran. [b]Reaction conditions: furfural 0.3 M; F/metal ratio = 500 mol/mol, 50 °C, 5 bar H_2, solvent 2-propranol. [c]Moles of furfural converted per hour per mole of metal, calculated after 15 min reaction: mol (metal mol)$^{-1}$ h^{-1}. [d]Selectivity at 60% conversion. [e]Selectivity at 10% conversion. [f]Calculated using 100 particles. A histogram is shown in Figure S7.

https://dx.doi.org/10.1021/acscatal.0c00414
ACS Catal. 2020, 10, 5483−5492

experiments confirmed that the dual-site hydrogenation mechanism found for Pd/NiO requires the intimate contact of both Pd and NiO.

The initial catalytic activity screening has found that Pd/NiO offers a unique dual-site mechanism for the hydrogenation of furfural. To investigate the catalyst further, a catalytic reusability study, over eight cycles, was performed (Figure 6). The reusability study found that there was an initial

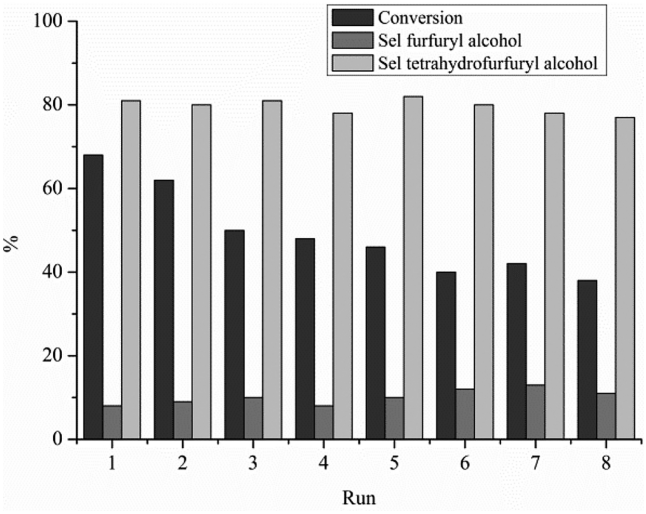

Figure 6. Reusability study for 1 wt % Pd/NiO detailing changes to conversion and selectivity over eight cycles (reaction time 5 h). Recycling experiments were performed by reusing the catalyst in the next run without any additional pretreatment.

reduction in the conversion of furfural, reducing from ~65 to 50% between the first and third runs, with a more gradual decline in conversion to ~40% by the eighth cycle. The final three catalytic screening cycles show a plateau region with no further reduction in catalytic activity. Throughout all the reusability studies, the selectivity to THFA remains broadly constant, indicating that the same mechanistic pathway dominates for every cycle. It has been established that the hydrogenation of furfural on Pd/TiO_2 deactivates through the formation of Pd carbide, which promotes a less advantageous adsorption of furfural.[18] To test if the formation of Pd carbide is responsible for this deactivation, ex situ X-ray absorption fine structure (XAFS) measurements were performed at the Pd K edge before and after catalytic testing (Figure 7).

The X-ray absorption near edge data (XANES) shown in Figure 7 demonstrate that the height of the main edge of the fresh Pd/NiO catalyst is greater than those of both the Pd foil and used Pd/NiO. This difference in height can be attributed to a greater degree of oxidized Pd in the fresh Pd/NiO catalyst. Small Pd nanoparticles have a high proportion of surface sites that readily adsorb oxygen on exposure to air. The height of the main edge for the used Pd/NiO catalyst is the same as that of the Pd foil, confirming the presence of Pd(0). There are two features in the XANES spectrum of the used Pd/NiO indicative of Pd carbide; there is a broadening of the first peak maximum and a shift to lower energy of the second peak maximum as a result of lattice expansion. The shift in the position of the second peak maximum is observed for both hydridic and carbidic forms of Pd; however, the broadening of the first peak is only observed for Pd carbide.[51,52] Furthermore, the insertion/removal of hydride into the Pd lattice is such that

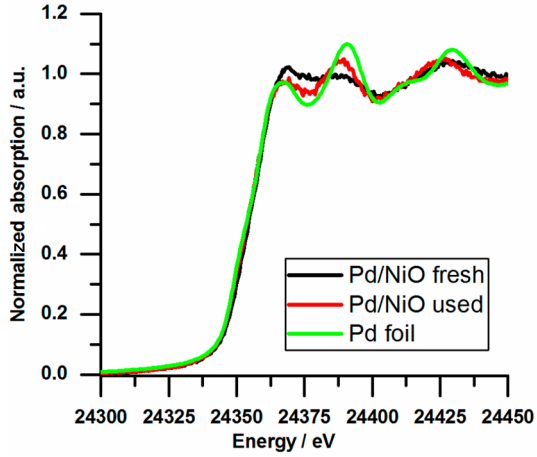

Figure 7. Pd K edge XANES of 1% Pd/NiO before and after reaction and a reference Pd foil.

without an overpressure of hydrogen present any incorporated hydride would quickly diffuse out from the Pd nanoparticle. The lack of oxygen coordination on the Pd surface, inferred from the XANES, is consistent with previous studies where heteroatoms are inserted into the Pd lattice.[53]

Analysis of the extended X-ray absorption fine structure (EXAFS) was also performed with the results shown in Table S1 and Figure 8. The EXAFS fitting parameters for the fresh Pd/NiO catalyst confirms that Pd is present as metallic Pd nanoparticles with an oxidized surface layer. There are no Pd−Pd scattering paths at longer distances, indicative of PdO, needed to model the data, and we can therefore discount the presence of large PdO crystallites. The EXAFS data for the used Pd/NiO catalyst can be modeled using a single Pd−Pd

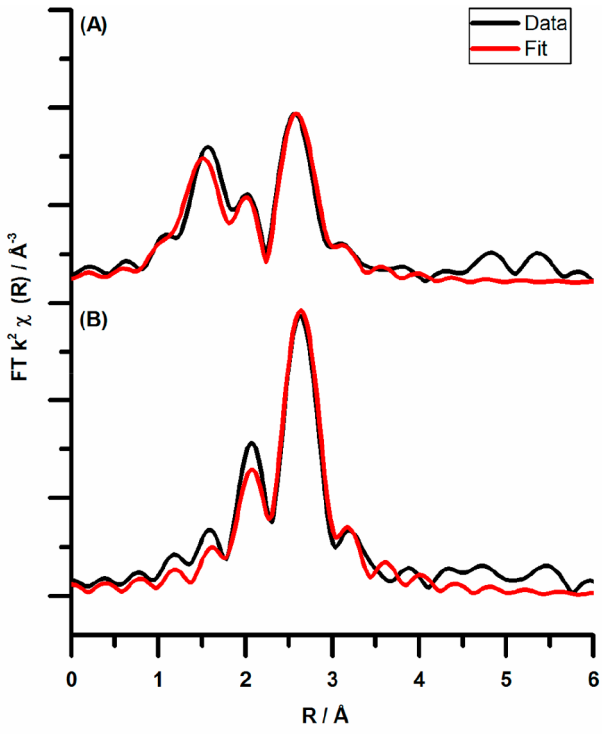

Figure 8. k^2-weighted Fourier transform EXAFS data with simulated fit for (a) the fresh Pd/NiO and (b) the used Pd/NiO.

https://dx.doi.org/10.1021/acscatal.0c00414
ACS Catal. 2020, 10, 5483−5492

scattering path. The expansion of the Pd lattice from 2.74 to2.79 Å is consistent with that previously reported for bulk Pd carbide formation.[51] The reduced Pd−Pd coordination number of the used Pd/NiO catalyst from 12 to 9 is indicative of small nanoparticles (<5 nm) of Pd.

The XAFS data confirm that there is a structural change during furfural hydrogenation on Pd/NiO that is consistent with the formation of Pd carbide. Previously, it has been shown that there is a less favorable binding of furfural on carbidic Pd, which is responsible for the loss of activity during reusability studies. However, in the case of Pd/NiO, it has been established that the activity arises from furfural adsorbed on the NiO surface. In this instance it is proposed that the loss of activity stems from the reduced ability of Pd carbide to dissociate hydrogen, which has also been found previously.[54]

CONCLUSION

This study reports a synergistic interaction between Pd NPs and NiO that is responsible for directing the selectivity of furfural hydrogenation, alongside being able to maintain catalytic activity at low Pd loading. This study proposes that the hydrogenation of furfural proceeds via a dual-site hydrogenation mechanism with the following steps: (i) hydrogen dissociation on Pd surfaces, (ii) spillover of H_{ads} onto the NiO support, (iii) parallel adsorption of furfural through both the furan ring and alcohol group onto the support, and (iv) hydrogenation of furfural on the NiO surface to yield THFA as the major product.

Initially, the nature of CO_{ads} on surfaces of Pd NPs through FTIR spectroscopy was used to assess the available catalytic sites. However, although there were subtle differences, the changes were not distinct enough to account for the different selectivity profiles of the 1 wt % Pd/TiO_2 and 1 wt % Pd/NiO samples. This led to the hypothesis that the NiO surface could be responsible for furfural adsorption and hydrogenation for the Pd/NiO catalyst. In this scenario, the role of Pd would be to dissociate hydrogen, which subsequently spills over onto the NiO support. Considering that hydrogen dissociation on Pd is a facile process and is unlikely to be rate limiting, we determined that the dual-site hydrogenation mechanism proposed could sustain similar activities at reduced Pd loading.

This assertion was confirmed by assessing the catalytic activity of 0.1 wt % Pd/NiO and 0.1 wt % Pd/TiO_2. With respect to their 1 wt % loading counterparts, the TiO_2-supported system showed an ∼10-fold reduction in catalytic activity. However, the activity of both NiO-supported catalysts was broadly similar.

The design strategy presented in this work can be extended to further substrates and is an important step in designing catalysts for the selective transformation of bioderived feedstocks that are less reliant on precious metals.

ASSOCIATED CONTENT

Supporting Information

The Supporting Information is available free of charge at https://pubs.acs.org/doi/10.1021/acscatal.0c00414.

Additional characterization data and details and images of the calculated structures (PDF

AUTHOR INFORMATION

Corresponding Authors

Peter P. Wells − *School of Chemistry, University of Southampton, Southampton SO17 1BJ, United Kingdom; Dipartimento di Chimica Industriale "Toso Montanari", Alma Mater Studiorum, University of Bologna, 40136 Bologna, Italy; UK Catalysis Hub, Research Complex at Harwell, Rutherford Appleton Laboratory, Didcot OX11 0FA, United Kingdom; Diamond Light Source Ltd., Harwell Science and Innovation Campus, Didcot OX11 0DE, United Kingdom*; Email: p.p.wells@soton.ac.uk

Alberto Villa − *Dipartimento di Chimica, Università degli Studi di Milano, 20133 Milano, Italy*; orcid.org/0000-0001-8656-6256; Email: alberto.villa@unimi.it

Authors

Sebastiano Campisi − *Dipartimento di Chimica, Università degli Studi di Milano, 20133 Milano, Italy*

Carine E. Chan-Thaw − *Dipartimento di Chimica, Università degli Studi di Milano, 20133 Milano, Italy*

Lidia E. Chinchilla − *McMaster University, Department of Materials Science and Engineering, Hamilton, Ontario L8S 4M, Canada*

Arunabhiram Chutia − *School of Chemistry, University of Lincoln, Lincoln LN6 7TS, United Kingdom*; orcid.org/0000-0002-5897-1729

Gianluigi A. Botton − *McMaster University, Department of Materials Science and Engineering, Hamilton, Ontario L8S 4M, Canada*; orcid.org/0000-0002-8746-1146

Khaled M. H. Mohammed − *School of Chemistry, University of Southampton, Southampton SO17 1BJ, United Kingdom; Department of Chemistry, Faculty of Science, Sohag University, Sohag, Egypt*

Nikolaos Dimitratos − *Dipartimento di Chimica Industriale "Toso Montanari", Alma Mater Studiorum, University of Bologna, 40136 Bologna, Italy*

Complete contact information is available at: https://pubs.acs.org/10.1021/acscatal.0c00414

Author Contributions

The manuscript was written through contributions of all authors. All authors have given approval to the final version of the manuscript.

Notes

The authors declare no competing financial interest.

All data supporting this study are openly available from the University of Southampton repository at https://doi.org/10.5258/SOTON/D1346.

ACKNOWLEDGMENTS

The authors wish to acknowledge Diamond Light Source for provision of the beamtime (SP10306). The RCaH are also acknowledged for use of facilities and support of their staff. A.C. acknowledges the use of Athena at HPC Midlands+ in this research, which was funded by the EPSRC (grant EP/P020232/1) via the EPSRC RAP call of spring 2018 and 2019. Supercomputer Wales is also thanked for the computing time. This work also used ARCHER—the UK National Supercomputing Service (http://www.archer.ac.uk) via the membership of the UK's HEC Materials Chemistry Consortium, which is funded by the EPSRC (EP/L000202). P.P.W. acknowledges the UK Catalysis Hub Consortium and EPSRC (Grants EP/

K014706/1, EP/K014668/1, EP/K014854/1, EP/K014714/1, and EP/I019693/1). P.P.W. and K.M.H.M. acknowledge the STFC GCRF START project for funding the position of K.M.H.M. (ST/R002754/1).

REFERENCES

(1) Huber, G. W.; Iborra, S.; Corma, A. Synthesis of Transportation Fuels from Biomass: Chemistry, Catalysts, and Engineering. *Chem. Rev.* **2006**, *106* (9), 4044−4098.
(2) Chheda, J. N.; Huber, G. W.; Dumesic, J. A. Liquid-Phase Catalytic Processing of Biomass-Derived Oxygenated Hydrocarbons to Fuels and Chemicals. *Angew. Chem., Int. Ed.* **2007**, *46* (38), 7164−7183.
(3) Besson, M.; Gallezot, P.; Pinel, C. Conversion of Biomass into Chemicals over Metal Catalysts. *Chem. Rev.* **2014**, *114* (3), 1827−1870.
(4) Dutta, S.; De, S.; Saha, B.; Alam, M. I. Advances in Conversion of Hemicellulosic Biomass to Furfural and Upgrading to Biofuels. *Catal. Sci. Technol.* **2012**, *2* (10), 2025−2036.
(5) Sitthisa, S.; Sooknoi, T.; Ma, Y.; Balbuena, P. B.; Resasco, D. E. Kinetics and Mechanism of Hydrogenation of Furfural on Cu/SiO2 Catalysts. *J. Catal.* **2011**, *277* (1), 1−13.
(6) Sitthisa, S.; Pham, T.; Prasomsri, T.; Sooknoi, T.; Mallinson, R. G.; Resasco, D. E. Conversion of Furfural and 2-Methylpentanal on Pd/SiO2 and Pd-Cu/SiO2 Catalysts. *J. Catal.* **2011**, *280* (1), 17−27.
(7) Yan, K.; Wu, G.; Lafleur, T.; Jarvis, C. Production, Properties and Catalytic Hydrogenation of Furfural to Fuel Additives and Value-Added Chemicals. *Renewable Sustainable Energy Rev.* **2014**, *38*, 663−676.
(8) Li, X.; Jia, P.; Wang, T. Furfural: A Promising Platform Compound for Sustainable Production of C4 and C5 Chemicals. *ACS Catal.* **2016**, *6* (11), 7621−7640.
(9) Nakagawa, Y.; Tamura, M.; Tomishige, K. Catalytic Reduction of Biomass-Derived Furanic Compounds with Hydrogen. *ACS Catal.* **2013**, *3* (12), 2655−2668.
(10) Iqbal, S.; Liu, X.; Aldosari, O. F.; Miedziak, P. J.; Edwards, J. K.; Brett, G. L.; Akram, A.; King, G. M.; Davies, T. E.; Morgan, D. J.; et al. Conversion of Furfuryl Alcohol into 2-Methylfuran at Room Temperature Using Pd/TiO2 Catalyst. *Catal. Sci. Technol.* **2014**, *4* (8), 2280−2286.
(11) Nakagawa, Y.; Nakazawa, H.; Watanabe, H.; Tomishige, K. Total Hydrogenation of Furfural over a Silica-Supported Nickel Catalyst Prepared by the Reduction of a Nickel Nitrate Precursor. *ChemCatChem* **2012**, *4* (11), 1791−1797.
(12) Rao, R. S.; Baker, R. T. K.; Vannice, M. A. Furfural Hydrogenation over Carbon-Supported Copper. *Catal. Lett.* **1999**, *60* (1−2), 51−57.
(13) Meng, X.; Yang, Y.; Chen, L.; Xu, M.; Zhang, X.; Wei, M. A Control over Hydrogenation Selectivity of Furfural via Tuning Exposed Facet of Ni Catalysts. *ACS Catal.* **2019**, *9*, 4226−4235.
(14) Seemala, B.; Cai, C. M.; Wyman, C. E.; Christopher, P. Support Induced Control of Surface Composition in Cu-Ni/TiO2 Catalysts Enables High Yield Co-Conversion of HMF and Furfural to Methylated Furans. *ACS Catal.* **2017**, *7* (6), 4070−4082.
(15) Sitthisa, S.; Resasco, D. E. Hydrodeoxygenation of Furfural over Supported Metal Catalysts: A Comparative Study of Cu, Pd and Ni. *Catal. Lett.* **2011**, *141* (6), 784−791.
(16) Schoenbaum, C. A.; Schwartz, D. K.; Medlin, J. W. Controlling the Surface Environment of Heterogeneous Catalysts Using Self-Assembled Monolayers. *Acc. Chem. Res.* **2014**, *47* (4), 1438−1445.
(17) Pang, S. H.; Schoenbaum, C. A.; Schwartz, D. K.; Medlin, J. W. Directing Reaction Pathways by Catalyst Active-Site Selection Using Self-Assembled Monolayers. *Nat. Commun.* **2013**, *4*, 2448.
(18) Palmer, R. E.; Jian, N.; Villa, A.; Dimitratos, N.; Catlow, C. R. A.; Chutia, A.; Wells, P. P.; Chan-Thaw, C. E.; Rogers, S. M.; Perdjon, M.; et al. Tandem Site- and Size-Controlled Pd Nanoparticles for the Directed Hydrogenation of Furfural. *ACS Catal.* **2017**, *7* (4), 2266−2274.
(19) Pang, S. H.; Schoenbaum, C. A.; Schwartz, D. K.; Medlin, J. W. Effects of Thiol Modifiers on the Kinetics of Furfural Hydrogenation over Pd Catalysts. *ACS Catal.* **2014**, *4* (9), 3123−3131.
(20) Pan, C. J.; Tsai, M. C.; Su, W. N.; Rick, J.; Akalework, N. G.; Agegnehu, A. K.; Cheng, S. Y.; Hwang, B. J. Tuning/Exploiting Strong Metal-Support Interaction (SMSI) in Heterogeneous Catalysis. *J. Taiwan Inst. Chem. Eng.* **2017**, *74*, 154−186.
(21) Tauster, S. J.; Fung, S. C.; Baker, R. T. K.; Horsley, J. A. Strong Interactions in Supported-Metal Catalysts. *Science (Washington, DC, U. S.)* **1981**, *211* (4487), 1121−1125.
(22) Campisi, S.; Chan-Thaw, C. E.; Villa, A. Understanding Heteroatom-Mediated Metal-Support Interactions in Functionalized Carbons: A Perspective Review. *Appl. Sci.* **2018**, *8* (7), 1159.
(23) Zhang, P.; Yuan, Q.; Chen, L.; Xue, T.; Guan, Y.; Wu, P. Low Temperature Hydrogenation of α-Angelica Lactone on Silica Supported Pd-NiO Catalysts with Synergistic Effect. *RSC Adv.* **2016**, *6* (70), 65377−65382.
(24) Villa, A.; Chan-Thaw, C. E.; Veith, G. M.; More, K. L.; Ferri, D.; Prati, L. Au on Nanosized NiO: A Cooperative Effect between Au and Nanosized NiO in the Base-Free Alcohol Oxidation. *ChemCatChem* **2011**, *3* (10), 1612−1618.
(25) Stoyanova, D.; Georgieva, P.; Kasabova, N. Pd-Containing Catalysts Promoted by NiO Designed for the Reduction of NO with CO at Stoichiometric NO/CO Ratio. *React. Kinet., Mech. Catal.* **2013**, *108* (2), 391−402.
(26) Bruix, A.; Rodriguez, J. A.; Ramírez, P. J.; Senanayake, S. D.; Evans, J.; Park, J. B.; Stacchiola, D.; Liu, P.; Hrbek, J.; Illas, F. A New Type of Strong Metal-Support Interaction and the Production of H 2 through the Transformation of Water on Pt/CeO 2(111) and Pt/CeO x/TiO 2(110) Catalysts. *J. Am. Chem. Soc.* **2012**, *134* (21), 8968−8974.
(27) He, J.; Nielsen, M. R.; Hansen, T. W.; Yang, S.; Riisager, A. Hierarchically Constructed NiO with Improved Performance for Catalytic Transfer Hydrogenation of Biomass-Derived Aldehydes. *Catal. Sci. Technol.* **2019**, *9* (5), 1289−1300.
(28) Baker, L. R.; Kennedy, G.; Van Spronsen, M.; Hervier, A.; Cai, X.; Chen, S.; Wang, L. W.; Somorjai, G. A. Furfuraldehyde Hydrogenation on Titanium Oxide-Supported Platinum Nanoparticles Studied by Sum Frequency Generation Vibrational Spectroscopy: Acid-Base Catalysis Explains the Molecular Origin of Strong Metal-Support Interactions. *J. Am. Chem. Soc.* **2012**, *134* (34), 14208−14216.
(29) Newville, M. IFEFFIT: Interactive XAFS Analysis and FEFF Fitting. *J. Synchrotron Radiat.* **2001**, *8* (2), 322−324.
(30) Ravel, B.; Newville, M. ATHENA, ARTEMIS, HEPHAESTUS: Data Analysis for X-Ray Absorption Spectroscopy Using IFEFFIT. *J. Synchrotron Radiat.* **2005**, *12* (4), 537−541.
(31) Kresse, G.; Hafner, J. Ab Initio Molecular Dynamics for Liquid Metals. *Phys. Rev. B: Condens. Matter Mater. Phys.* **1993**, *47* (1), 558−561.
(32) Kresse, G.; Furthmüller, J. Efficient Iterative Schemes for Ab Initio Total-Energy Calculations Using a Plane-Wave Basis Set. *Phys. Rev. B: Condens. Matter Mater. Phys.* **1996**, *54* (16), 11169−11186.
(33) Kresse, G.; Hafner, J. Ab Initio Molecular-Dynamics Simulation of the Liquid-Metalamorphous- Semiconductor Transition in Germanium. *Phys. Rev. B: Condens. Matter Mater. Phys.* **1994**, *49* (20), 14251−14269.
(34) Blöchl, P. E. Projector Augmented-Wave Method. *Phys. Rev. B: Condens. Matter Mater. Phys.* **1994**, *50* (24), 17953−17979.
(35) Perdew, J. P.; Burke, K.; Ernzerhof, M. Generalized Gradient Approximation Made Simple. *Phys. Rev. Lett.* **1996**, *77* (18), 3865−3868.
(36) Grimme, S.; Antony, J.; Ehrlich, S.; Krieg, H. A Consistent and Accurate Ab Initio Parametrization of Density Functional Dispersion Correction (DFT-D) for the 94 Elements H-Pu. *J. Chem. Phys.* **2010**, *132* (15), 154104.
(37) Makov, G.; Payne, M. C. Periodic Boundary Conditions in Ab Initio Calculations. *Phys. Rev. B: Condens. Matter Mater. Phys.* **1995**, *51* (7), 4014−4022.

https://dx.doi.org/10.1021/acscatal.0c00414
ACS Catal. 2020, 10, 5483−5492

(38) Neugebauer, J.; Scheffler, M. Adsorbate-Substrate and Adsorbate-Adsorbate Interactions of Na and K Adlayers on Al(111). *Phys. Rev. B: Condens. Matter Mater. Phys.* **1992**, *46* (24), 16067−16080.
(39) Himmetoglu, B.; Floris, A.; De Gironcoli, S.; Cococcioni, M. Hubbard-Corrected DFT Energy Functionals: The LDA+U Description of Correlated Systems. *Int. J. Quantum Chem.* **2014**, *114* (1), 14−49.
(40) Morgan, B. J.; Watson, G. W. A DFT + U Description of Oxygen Vacancies at the TiO2 Rutile (1 1 0) Surface. *Surf. Sci.* **2007**, *601* (21), 5034−5041.
(41) Rogers, S. M.; Catlow, C. R. A.; Chan-Thaw, C. E.; Gianolio, D.; Gibson, E. K.; Gould, A. L.; Jian, N.; Logsdail, A. J.; Palmer, R. E.; Prati, L.; et al. Tailoring Gold Nanoparticle Characteristics and the Impact on Aqueous-Phase Oxidation of Glycerol. *ACS Catal.* **2015**, *5* (7), 4377−4384.
(42) Soma-Noto, Y.; Sachtler, W. M. H. Infrared Spectra of Carbon Monoxide Adsorbed on Supported Palladium and Palladium-Silver Alloys. *J. Catal.* **1974**, *32* (2), 315−324.
(43) Lear, T.; Marshall, R.; Lopez-Sanchez, J. A.; Jackson, S. D.; Klapötke, T. M.; Bäumer, M.; Rupprechter, G.; Freund, H. J.; Lennon, D. The Application of Infrared Spectroscopy to Probe the Surface Morphology of Alumina-Supported Palladium Catalysts. *J. Chem. Phys.* **2005**, *123* (17), 174706.
(44) Vesecky, S. M.; Xu, X.; Goodman, D. W. Infrared Study of CO on NiO(100). *J. Vac. Sci. Technol., A* **1994**, *12* (4), 2114−2118.
(45) Hadjiivanov, K. I.; Vayssilov, G. N. Characterization of Oxide Surfaces and Zeolites by Carbon Monoxide as an IR Probe Molecule. *Adv. Catal.* **2002**, *47*, 307−511.
(46) Wang, S.; Vorotnikov, V.; Vlachos, D. G. Coverage-Induced Conformational Effects on Activity and Selectivity: Hydrogenation and Decarbonylation of Furfural on Pd(111). *ACS Catal.* **2015**, *5* (1), 104−112.
(47) Vorotnikov, V.; Mpourmpakis, G.; Vlachos, D. G. DFT Study of Furfural Conversion to Furan, Furfuryl Alcohol, and 2-Methylfuran on Pd(111). *ACS Catal.* **2012**, *2* (12), 2496−2504.
(48) Liu, B.; Cheng, L.; Curtiss, L.; Greeley, J. Effects of van Der Waals Density Functional Corrections on Trends in Furfural Adsorption and Hydrogenation on Close-Packed Transition Metal Surfaces. *Surf. Sci.* **2014**, *622*, 51−59.
(49) Huang, X.; Ouyang, X.; Hendriks, B. M. S.; Gonzalez, O. M. M.; Zhu, J.; Korányi, T. I.; Boot, M. D.; Hensen, E. J. M. Selective Production of Mono-Aromatics from Lignocellulose over Pd/C Catalyst: The Influence of Acid Co-Catalysts. *Faraday Discuss.* **2017**, *202*, 141−156.
(50) Chutia, A.; Thetford, A.; Stamatakis, M.; Catlow, C. R. A. A DFT and KMC Based Study on the Mechanism of Water Gas Shift Reaction on Pd(100) Surface. *Phys. Chem. Chem. Phys.* **2020**, *22*, 3620.
(51) McCaulley, J. A. Temperature Dependence of the Pd K-Edge Extended x-Ray-Absorption Fine Structure of PdCx (X ∼ 0.13). *Phys. Rev. B: Condens. Matter Mater. Phys.* **1993**, *47* (9), 4873−4879.
(52) Wells, P. P.; Crabb, E. M.; King, C. R.; Wiltshire, R.; Billsborrow, B.; Thompsett, D.; Russell, A. E. Preparation, Structure, and Stability of Pt and Pd Monolayer Modified Pd and Pt Electrocatalysts. *Phys. Chem. Chem. Phys.* **2009**, *11* (27), 5773−5781.
(53) Dann, E. K.; Gibson, E. K.; Blackmore, R. H.; Catlow, C. R. A.; Collier, P.; Chutia, A.; Erden, T. E.; Hardacre, C.; Kroner, A.; Nachtegaal, M.; et al. Structural Selectivity of Supported Pd Nanoparticles for Catalytic NH 3 Oxidation Resolved Using Combined Operando Spectroscopy. *Nat. Catal.* **2019**, *2* (2), 157−163.
(54) Armbrüster, M.; Behrens, M.; Cinquini, F.; Föttinger, K.; Grin, Y.; Haghofer, A.; Klötzer, B.; Knop-Gericke, A.; Lorenz, H.; Ota, A.; et al. How to Control the Selectivity of Palladium-Based Catalysts in Hydrogenation Reactions: The Role of Subsurface Chemistry. *ChemCatChem* **2012**, *4* (8), 1048−1063.

https://dx.doi.org/10.1021/acscatal.0c00414
ACS Catal. 2020, 10, 5483−5492

Supporting information

Dual-Site Mediated Hydrogenation Catalysis on Pd/NiO: Selective Biomass Transformation and Maintaining Catalytic Activity at Low Pd Loading.

Sebastiano Campisi[†], Carine E. Chan-Thaw[†], Lidia E. Chinchilla[‡], Arunabhiram Chutia[#], Gianluigi A. Botton[‡], Khaled. M. H. Mohammed[§,¢], Nikolaos Dimitratos[¥], Peter P. Wells[§,◊,○*] and Alberto Villa[†*]

† Dipartimento di Chimica, Università degli Studi di Milano, via Golgi 19, 20133 Milano, Italy.

‡ McMaster University, Department of Materials Science and Engineering, Hamilton, Ontario, L8S 4M, Canada.

School of Chemistry, University of Lincoln, Lincoln, LN6 7TS.

§ School of Chemistry, University of Southampton, University Road, Southampton, SO17 1BJ, United Kingdom.

¢ Department of Chemistry, Faculty of Science, Sohag University, Sohag, P.O.Box 82524, Egypt.

¥ Dipartimento di Chimica Industriale "Toso Montanari", Alma Mater Studiorum, University of Bologna, Viale Risorgimento 4, 40136, Bologna, Italy.

◊ UK Catalysis Hub, Research Complex at Harwell, Rutherford Appleton Laboratory, Harwell Oxon, Didcot, OX11 0FA.

○ Diamond Light Source Ltd., Harwell Science and Innovation Campus, Chilton, Didcot OX11 0DE, United Kingdom.

Corresponding Author

* Email: p.p.wells@soton.ac.uk.
* Email: alberto.villa@unimi.it.

Figure S1. XRD patterns of NiO.

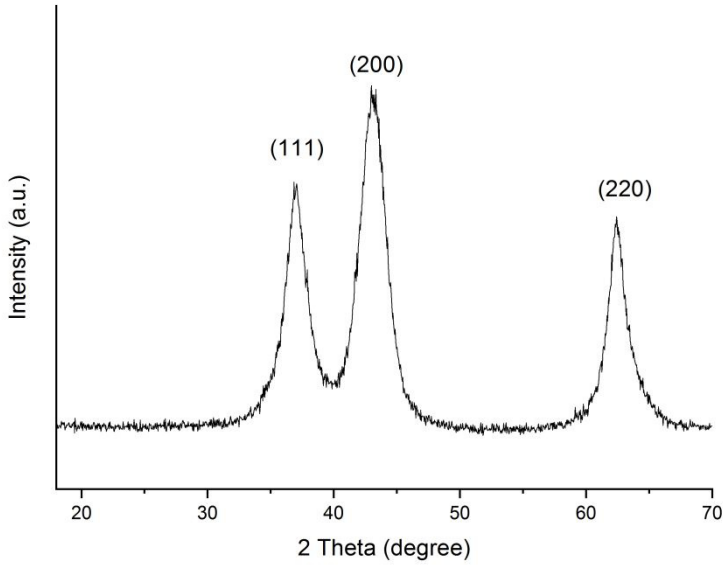

Figure S2. Pd 3d XPS data for (a) Pd/NiO, (b) Pd/TiO_2 and (c) Ni2p3/2 XPS data for NiO.

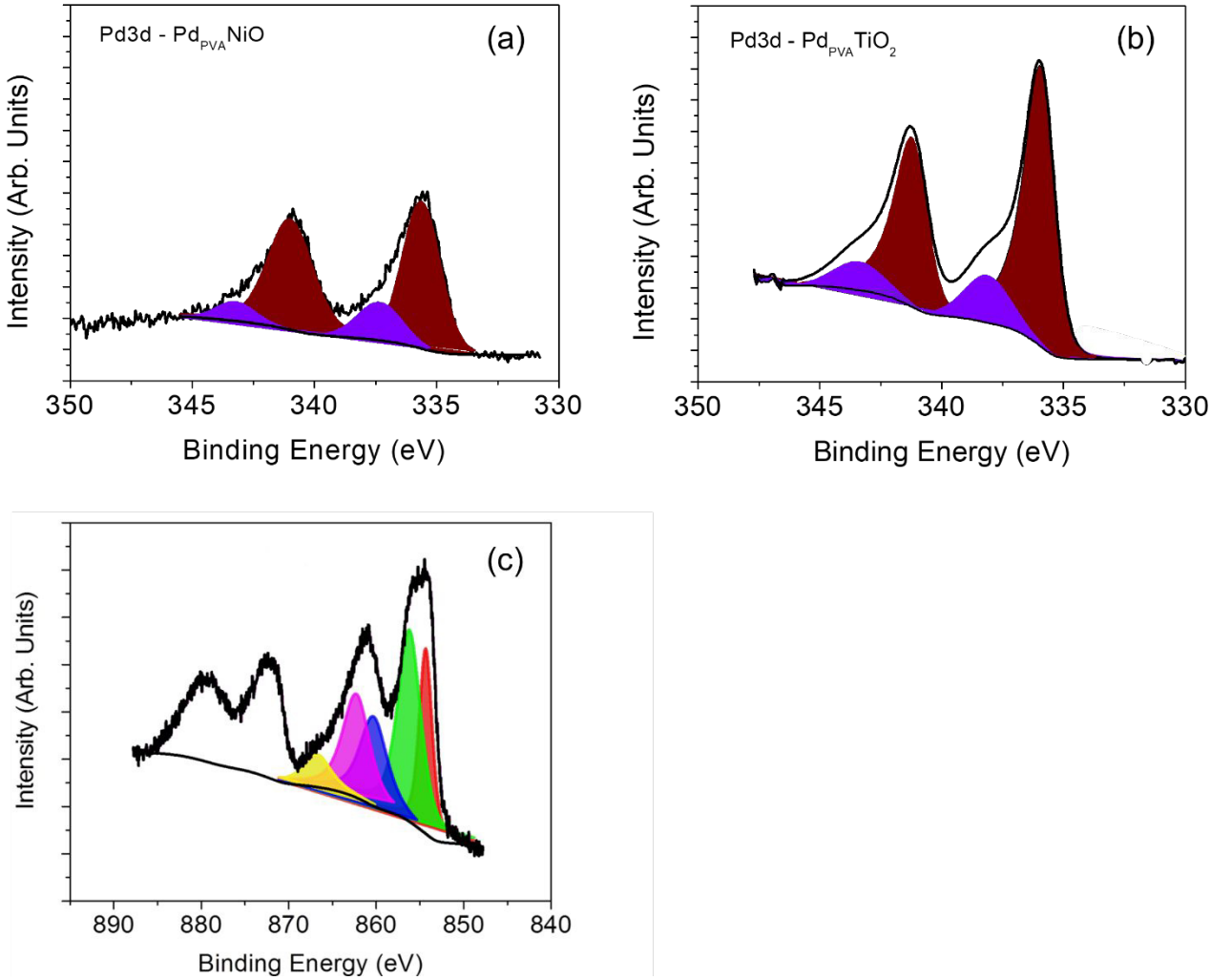

Figure S3. Reaction profile for 1 wt% Pd/TiO_2 and b) 1 wt% Pd/NiO.

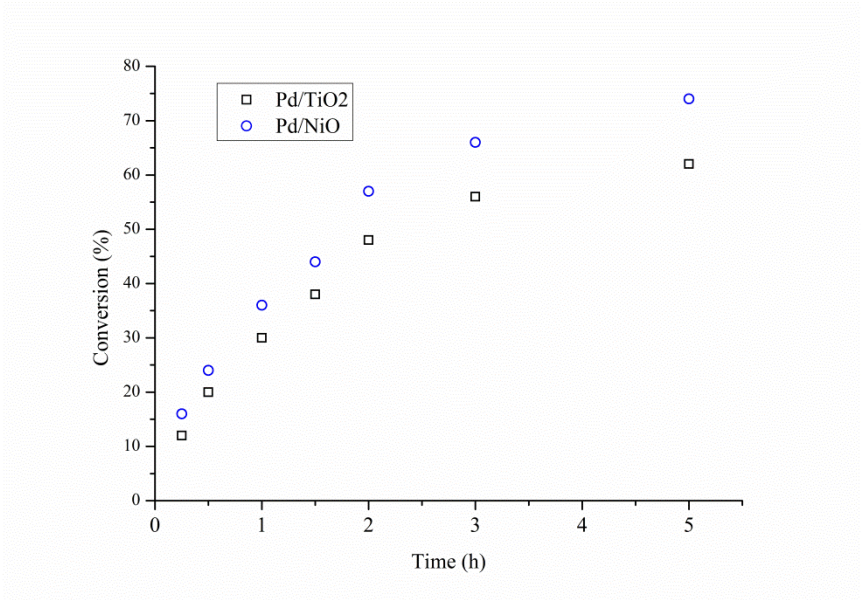

Figure S4. Selectivity vs conversion for a) 1 wt% Pd/TiO_2 and b) 1 wt% Pd/NiO.

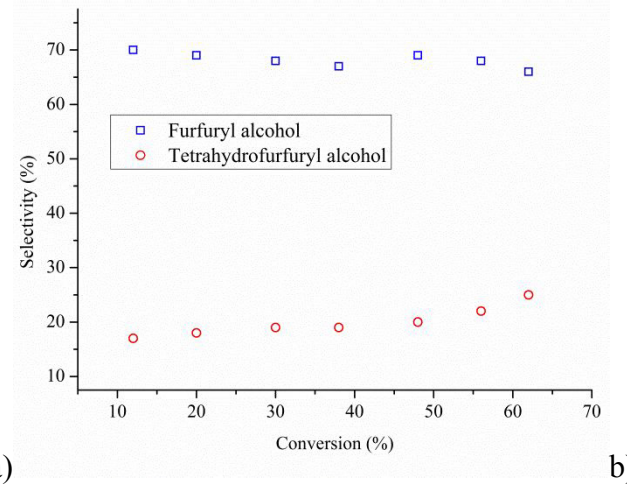

a)

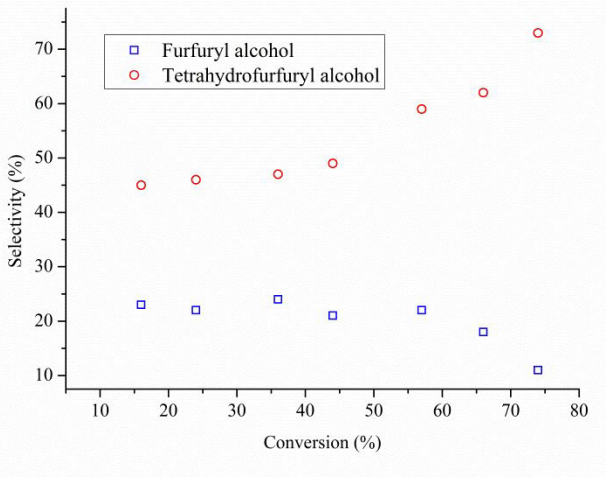

b)

Figure S5. Particle size distribution for a) 1 wt% Pd/TiO_2 and b) 1wt% Pd/NiO.

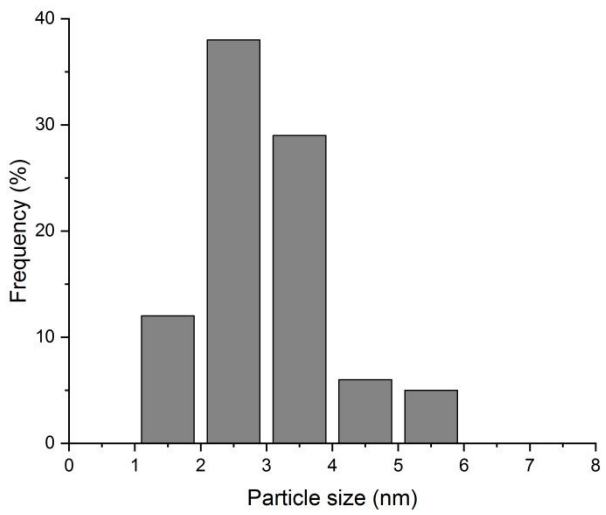

a)

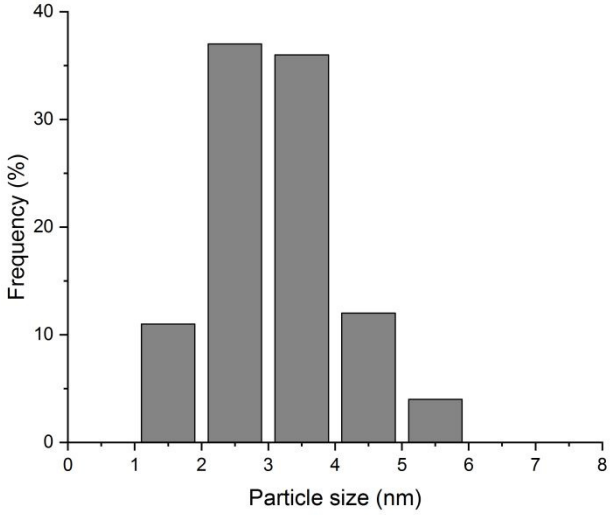

b)

Figure S6. High resolution STEM-HAADF images of 1 wt% Pd/NiO catalyst showing a crystalline particle (a) and sub nanometer species of Pd distributed across the support (b). Results of EELS-SI measurement, showing the HAADF image (c) and artificially colored overlay of Pd (green) and NiO (pink) maps (d). Bottom are independent components spectra and their corresponding distribution determined through machine learning methods implemented in Hyperspy.

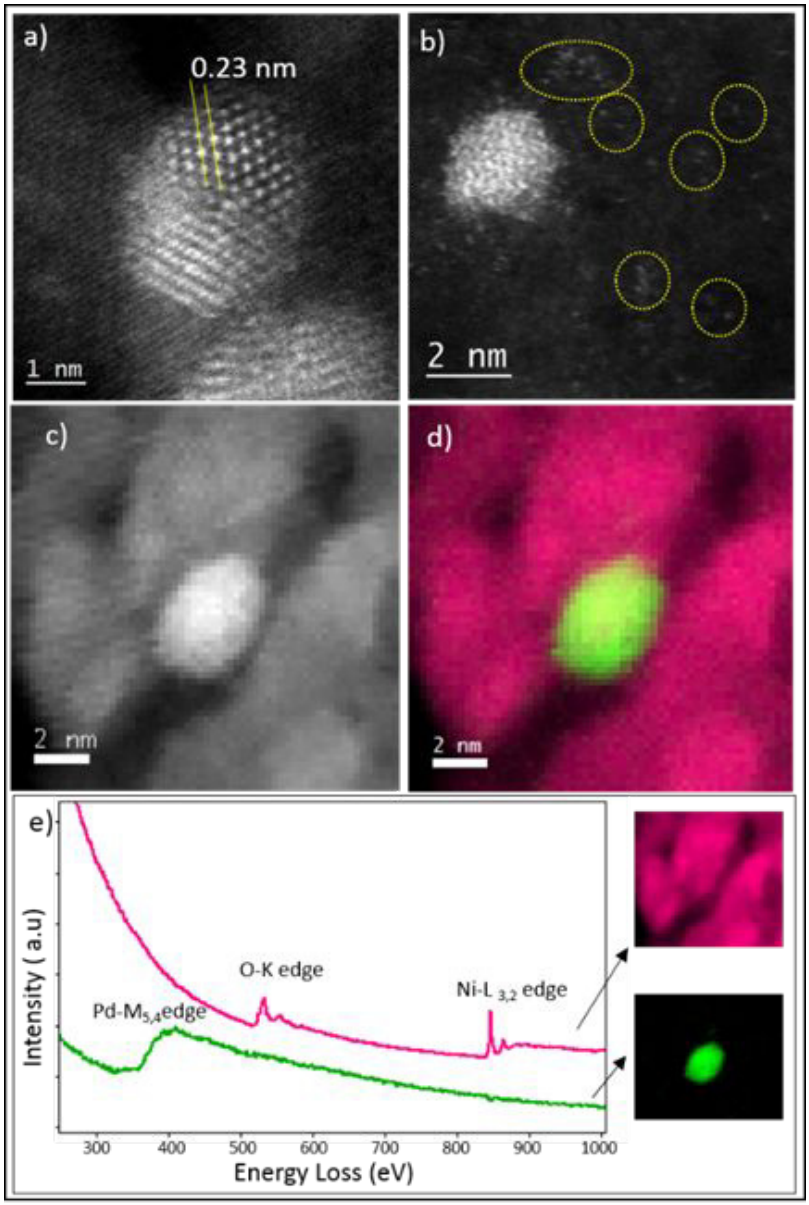

Figure S7. Optimized geometries of perpendicular configurations of furfural on (a) top of Pd atom (Pd_{top}), (b) bridge between to Pd-atoms (Pd_{bdg}), and (c) hollow site in-between three Pd-atoms (Pd_{hollow}). The optimized geometries of parallel configurations of furfural on Pd(111) (d) Conf.1, (e) Conf.2 and (f) Conf.3.

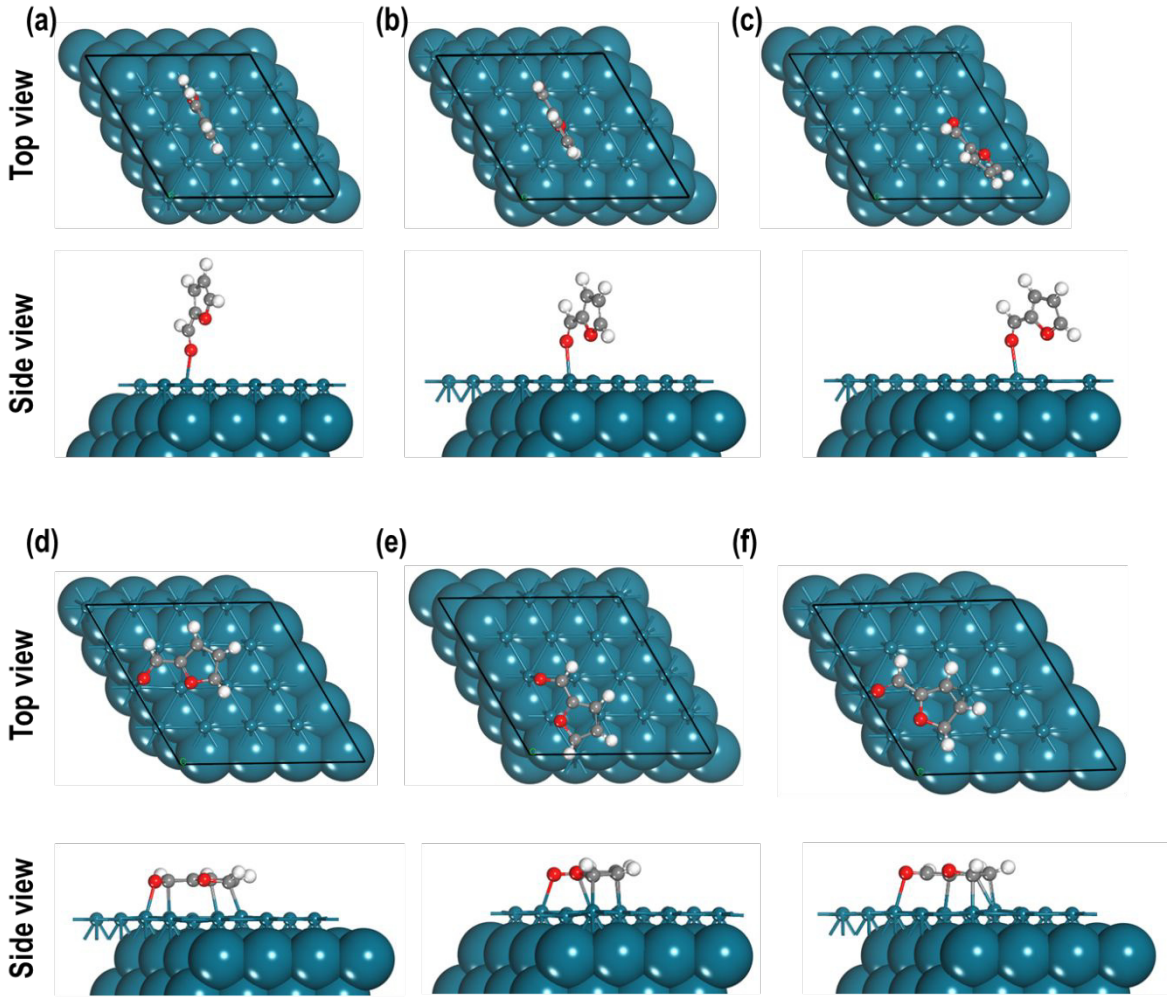

Figure S8. Optimized geometries of (a) NiO_conf1, (b) NiO_conf2, (c) NiO_conf3, (d) NiO_conf4, (e) NiO_conf5, (f) NiO_conf6, (g) NiO_conf7, (h) NiO_conf8, (i) NiO_conf9, (j) NiO_conf10, (k) NiO_conf11, (l) NiO_conf12, (m) NiO_conf13, (n) NiO_conf14, (o) NiO_conf15, (p) NiO_conf16, (q) NiO_conf17, (r) NiO_conf18, (s) NiO_conf19.

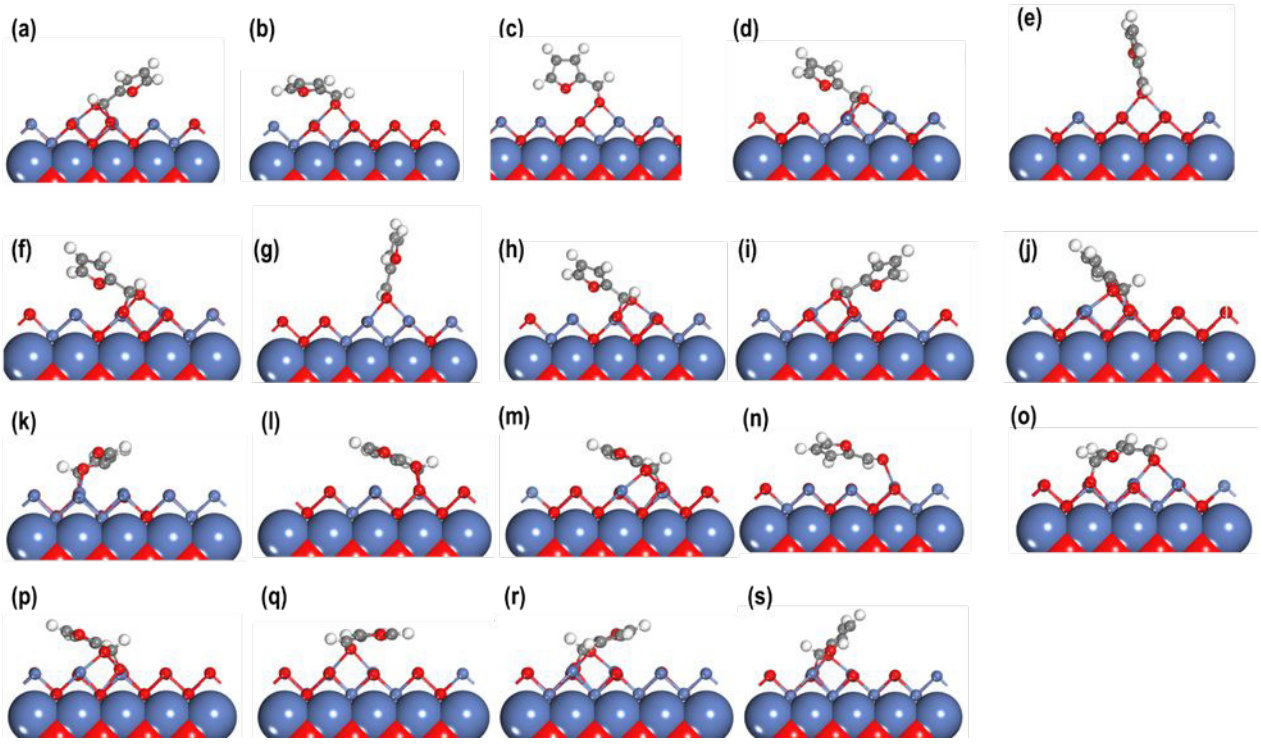

Figure S9. Optimized geometries of (a) TiO_2_conf1, (b) TiO_2_conf2, (c) TiO_2_conf3, (d) TiO_2_conf4, (e) TiO_2_conf5, (f) TiO_2_conf6, (g) TiO_2_conf7, (h) TiO_2_conf8, (i) TiO_2_conf9, and (j) TiO_2_conf10.

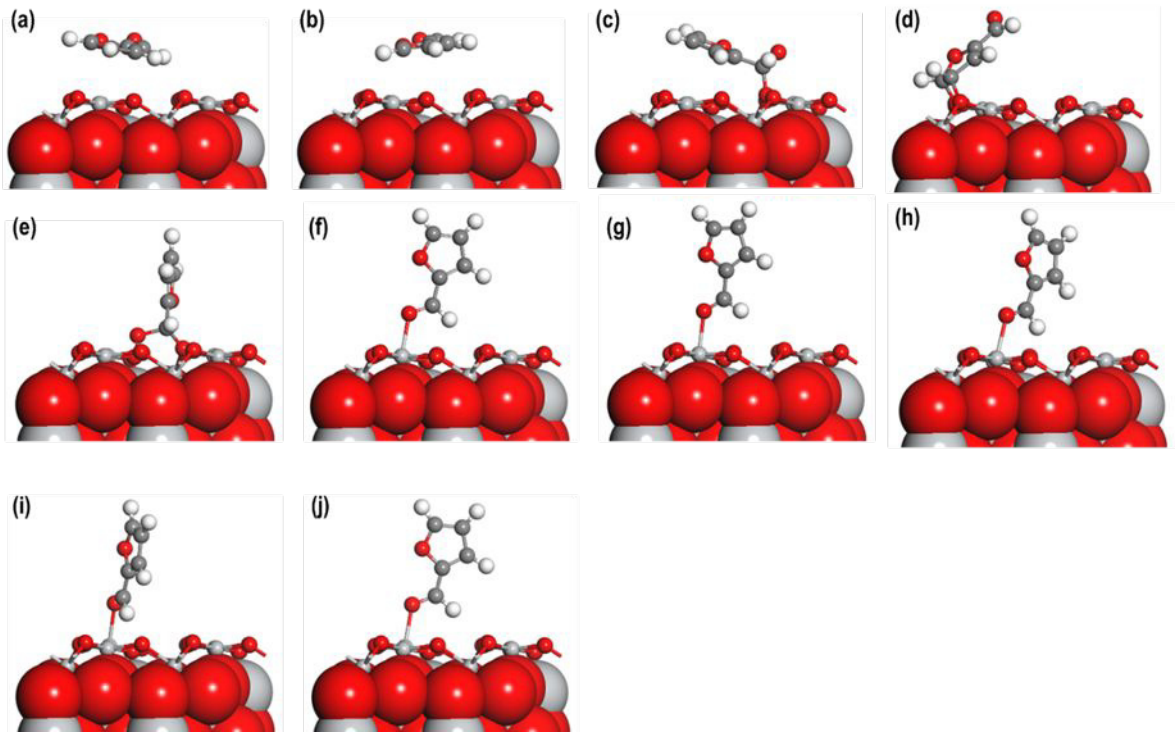

Figure S10. Optimised structures of (a) furfural parallel (E_{ad} = -1.946 eV), (b) furfural on top of Pd-atom (E_{ad} = -0.396 eV), (c) furfural in between two Pd-atoms (E_{ad} = -0.964 eV), (d) furfural in the HCP (E_{ad} = -1.017 eV) site of Pd_{16}-NiO(110) systems.

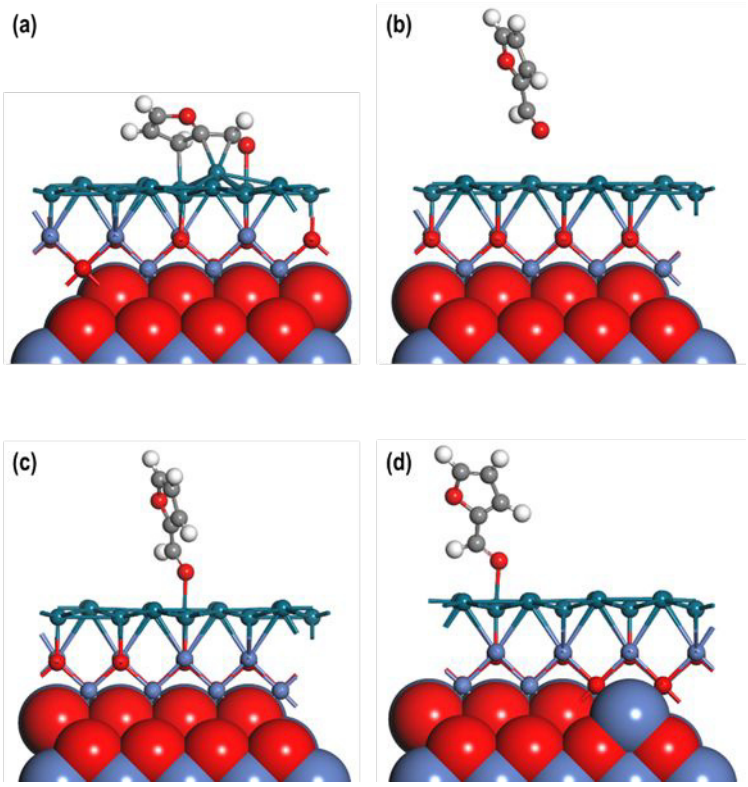

Figure S11. The energy barrier for the for the forward and reverse reaction of H_2 dissociation.

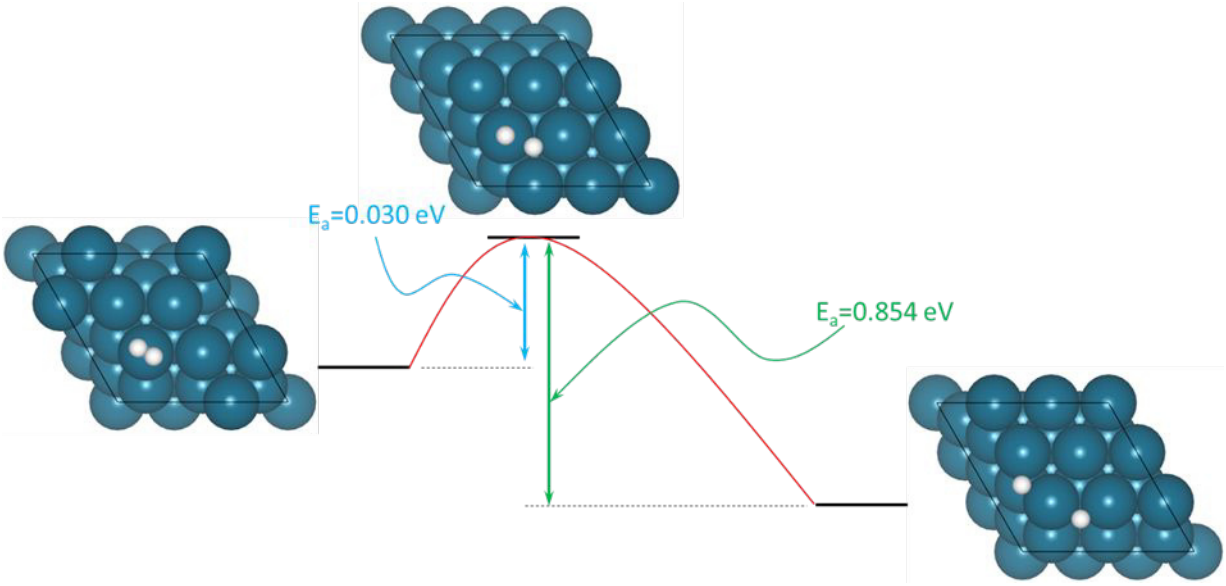

Figure S12. Particle size distribution for a) 0.1 wt% Pd/TiO_2 and b) 0.1 wt% Pd/NiO.

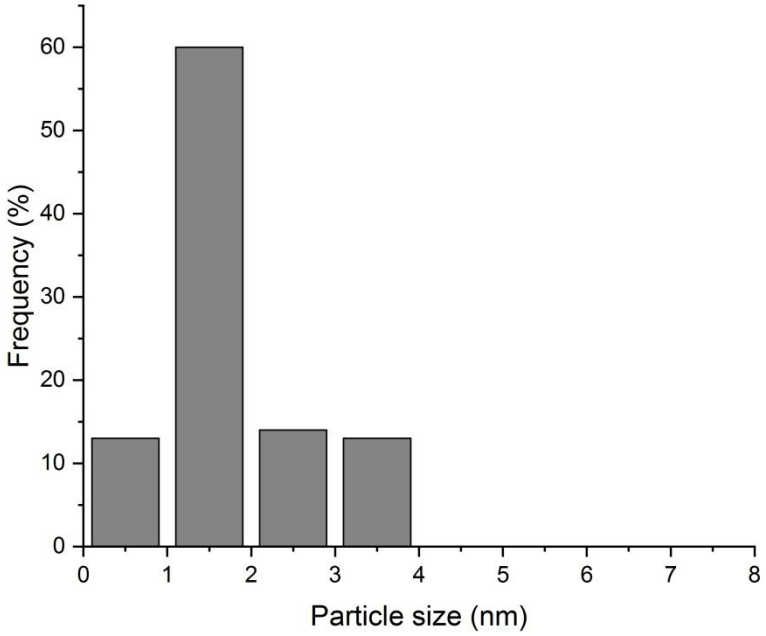

a)

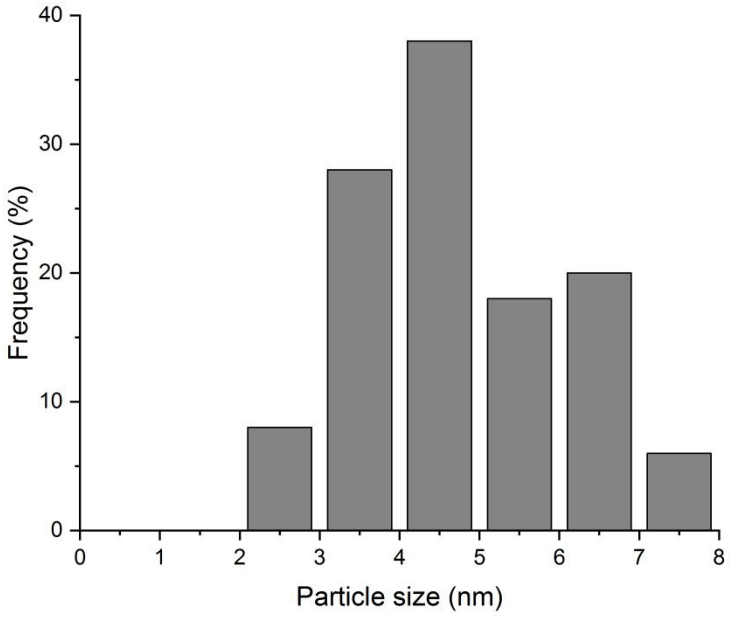

b)

Table S1. Furfural hydrogenation at 50 °C using 1 wt% Pd/NiO: influence of catalyst amount.

F/Metal ratio[a]	Activity[b] mol (metal mol)$^{-1}$ h^{-1}	Selectivity (%)[c]						
		Furfuryl alcohol	Tetrahydro Furfuryl Alcohol	2-methyl furan	2-methyl tetrahydro Furan	Furan	Ethers 1	Ethers 2
1/250	480	9	78	-	7	-	-	5
1/500	470	14	72	1	5	1	-	3
1/1000	485	21	65	-	3	-	3	2

[a] Reaction conditions: Furfural = 0.3 M, 50 °C, 5 bar H_2, solvent 2-propranol
[b] Mol of furfural converted per hour per mol of metal, calculated after 15 min reaction
[c] Selectivity at 60% conversion
[d] Selectivity at 10% conversion

Table S2. The calculated adsorption energies of 19 different models used to investigate the interaction of furfural on NiO(100) surface. The orientation of the initial and final geometry followed by the nature of interaction between furfural and NiO(100) has been also summarised.

System	Orientation		Bonded	Ead
	Initial	Final	through	
NiO_conf1	Perpendicular	Slanted	Aldehyde O & C	-2.218
NiO_conf2		Slanted	Aldehyde O	-1.579
NiO_conf3		Perpendicular	Aldehyde O	-1.280
NiO_conf4		Slanted	Aldehyde O & C	-2.319
NiO_conf5		Perpendicular	Aldehyde O	-1.151
NiO_conf6		Slanted	Aldehyde O & C	-2.345
NiO_conf7		Perpendicular	Aldehyde O	-1.152
NiO_conf8		Slanted	Aldehyde O & C	-2.290
NiO_conf9	Parallel	Slanted	Aldehyde O & C	-2.322
NiO_conf10		Slanted	Aldehyde O & C Furanic O	-2.572
NiO_conf11		Slanted	Furanic O & C	-1.075
NiO_conf12		Slanted	Aldehyde C	-2.291
NiO_conf13		Slanted	Aldehyde O & C	-2.405
NiO_conf14		Slanted	Aldehyde O	-1.149
NiO_conf15		Parallel distorted	Aldehyde O Furanic C	-2.013
NiO_conf16		Slanted	Aldehyde O & C	-2.405
NiO_conf17		Slanted	Aldehyde O	-1.601
NiO_conf18		Slanted	Aldehyde O & C	-2.404
NiO_conf19		Slanted	Aldehyde O & C Furanic O	-2.449

The systems in which the furfural molecule is adsorbed via aldehydic O and C and the O-atom in the furanic ring was seen to be most stable.

Table S3. The orientation of furfural before and after relaxation followed by the nature of interaction after relaxation and the adsorption energies in different models of furfural on TiO_2(111) surface.

System	orientation		Bonded through	Ead
	Initial	Final		
TiO_2_conf1	parallel	slightly slanted	None	-0.963
TiO_2_conf2		slightly slanted	None	-0.796
TiO_2_conf3		slanted	C of CHO	-0.484
TiO_2_conf4		slanted	C of furanic ring to O	-4.113
TiO_2_conf5			C and O of CHO to O	-1.633
TiO_2_conf6	perpendicular	perpendicular	O of CHO to Ti	-1.138
TiO_2_conf7			O of CHO to Ti	-1.061
TiO_2_conf8			O of CHO to Ti	-1.187
TiO_2_conf9			O of CHO to Ti	-1.056
TiO_2_conf10			O of CHO to Ti	-1.126